Am J Physiol Regul Integr Comp Physiol 292: R2340–R2351, 2007.
First published March 1, 2007; doi:10.1152/ajpregu.00905.2006.

Gene cloning and expression of an aquaporin (AQP-h3BL) in the basolateral membrane of water-permeable epithelial cells in osmoregulatory organs of the tree frog

Gen Akabane,[1] Yuji Ogushi,[1] Takahiro Hasegawa,[1] Masakazu Suzuki,[1] and Shigeyasu Tanaka[1,2]

[1]*Department of Biology, Faculty of Science and* [2]*Integrated Bioscience Section, Graduate School of Science and Technology, Shizuoka University, Shizuoka, Japan*

Submitted 28 December 2006; accepted in final form 15 February 2007

Akabane G, Ogushi Y, Hasegawa T, Suzuki M, Tanaka S. Gene cloning and expression of an aquaporin (AQP-h3BL) in the basolateral membrane of water-permeable epithelial cells in osmoregulatory organs of the tree frog. *Am J Physiol Regul Integr Comp Physiol* 292: R2340–R2351, 2007. First published March 1, 2007; doi:10.1152/ajpregu.00905.2006.—An aquaporin (Hyla AQP-h3BL), consisting of 292 amino acid residues, has been cloned from the urinary bladder of *Hyla japonica*. In a swelling assay using *Xenopus* oocytes, AQP-h3BL cRNA-injected oocytes developed a sevenfold and 2.8-fold higher permeability to water and glycerol, respectively, than the water-injected oocytes. This permeability was inhibited by $HgCl_2$. Immunofluorescence revealed that AQP-h3BL is localized in the basolateral plasma membrane of both granular cells in the ventral pelvic and dorsal skins and the secretory cells in the mucous glands. Immunopositive cells were also observed in the basolateral membrane of principal cells in the collecting ducts and in a portion of the late distal tubules in the kidneys, as well as in the principal cells of the urinary bladder. Sequence homology suggests that AQP-h3BL is a homolog to mammalian AQP3. This conclusion is supported by the observed localization of AQP-h3BL to the basolateral membrane in water- and glycerol-permeable epithelial cells. In ventral pelvic skins and urinary bladders, water enters into the cytoplasm through the apical plasma membrane at sites where AQP-h2, sometimes in association with AQP-h3, responds to stimulation by vasotocin; the water exits throughout AQP-h3BL to extracellular spaces. In the mucous glands, on the other hand, water enters throughout this AQP-h3BL and exits through AQP-x5, which is in the apical membrane of secretory cells. Thus, water homeostasis in the frog body is regulated by AQP-h3BL expressed in the basolateral membrane in concert with arginine vasotocin (AVT)-dependent or AVT-independent AQP.

skin; urinary bladder; kidney; mucous gland; arginine vasotocin; immunocytochemistry; anuran amphibian

PRESENT-DAY AMPHIBIANS ARE representative of the first vertebrates that made the transition from aquatic habitats to terrestrial environments. To adapt to these drier environments, many adult anurans have evolved specialized osmoregulatory organs that consist of a ventral pelvic skin capable of absorbing water from the external environment and a urinary bladder that stores water and reabsorbs it in times of need. The neurohypophyseal hormone arginine vasotocin (AVT), the nonmammalian vertebrate counterpart of vasopressin, stimulates these organs, thereby facilitating water absorption in many anuran species (2). The classic concept of this process was diffusion of water through the lipid bilayer of plasma membrane. However, biophysical and physiological studies predicted that water movement occurs through membrane channel proteins (3), and during the early 1990s, such water channel proteins were indeed discovered. These were given the name aquaporins (AQPs) (1), and they have been subsequently identified in many organisms, ranging from bacteria to plants and animals (19, 29). AQPs form membrane pores that are selectively permeable to water, but there is a subfamily of AQPs, termed aquaglyceroporins, comprising membrane pores that are permeated by certain small solutes, such as glycerol and urea. In mammals, 13 isoforms of AQPs (AQP0-AQP12) have been identified and characterized by cloning and sequencing of their cDNA (19, 32).

We have previously cloned cDNAs encoding three distinct AQPs (AQP-h1, AQP-h2, and AQP-h3) from the ventral pelvic skin of the tree frog, *Hyla japonica* (12, 35). AQP-h1 was found to be homlogous to mammalian AQP1 and showed a ubiquitous tissue distribution, AQP-h2 protein was expressed in the ventral pelvic skin and urinary bladder but not in the kidney, whereas AQP-h3 displayed a specific distribution that was restricted to the ventral pelvic skins. Empirical evidence has shown that following the stimulation of AVT secretion, water is absorbed from the apical plasma membrane of granular cells in the ventral pelvic cells and the urinary bladder through the mediation of AQP-h2 together with AQP-h3, or by AQP-h2 alone, respectively (12, 14). However, to date, no information is available on AQPs being involved in the exit of water through the basolateral plasma membranes of these tissues in these frogs. Our hypothesis is that some kind of AQP is expressed in the basolateral plasma membrane of granular cells in the ventral skins and urinary bladders.

Mammalian AQP3 exhibits a homology to the glycerol facilitator protein (GlpF) of *Escherichia coli* (6, 17, 24) and is expressed specifically in water-permeable epithelial tissues, including the kidney collecting ducts (7, 27) where it is localized at the basolateral plasma membrane of the principal cells (7, 17, 24). AQP2, on the other hand, resides in the intracellular vesicles and moves to the apical plasma membranes in response to vasopressin (28, 39). Working in concert with AQP2 at the apical membrane, AQP3 at the basolateral membrane mediates in the exit of water from the cell to the connective tissue in the transepithelial transfer of water across the principal cells of the kidney collecting duct (8, 17).

We report here the identification of a new member of the amphibian AQP family, AQP-h3BL, which we have isolated

Address for reprint requests and other correspondence: S. Tanaka, Integrated Bioscience Section, Graduate School of Science and Technology, Shizuoka Univ., Ohya 836, Shizuoka 422-8529, Japan (e-mail: sbstana@ipc.shizuoka.ac.jp).

The costs of publication of this article were defrayed in part by the payment of page charges. The article must therefore be hereby marked "*advertisement*" in accordance with 18 U.S.C. Section 1734 solely to indicate this fact.

from the urinary bladder of *H. japonica*. AQP-h3BL shows a high amino acid sequence homology to mammalian AQP3 and is predominately expressed in the basolateral plasma membrane of several osmoregulatory tissues, including skins, urinary bladders, and kidneys.

MATERIALS AND METHODS

Animals

Adult tree frogs (*H. japonica*) were captured in a field near our university (Shizuoka University, Shizuoka, Japan), kept under laboratory conditions, and fed crickets. The urinary bladders were removed from anesthetized animals (MS 222; Nacalai Tesque, Kyoto, Japan) for processing and subsequent use in cDNA cloning experiments. The animals were then killed, and various tissues (the ventral skin, dorsal skin, urinary bladder, kidney, heart, small intestine, lung, liver, and brain) were removed for analysis by Western blot and immunocytochemistry. All animal experiments were carried out in compliance with the "Guide for Care and Use of Laboratory Animals" of Shizuoka University.

Oligonucleotide Design

Oligonucleotide primers for the amplification of Hyla AQP-h3BL were designed based on the conserved region of other species. The sense primer and antisense primer used for cloning Hyla AQP-h3BL are given in Table 1.

Cloning of the Partial-Length cDNA

Urinary bladders were used for total RNA preparation. These urinary bladders were dissected out of anesthetized animals and frozen in liquid nitrogen; total RNA was extracted with Trizol RNA extraction reagent (Invitrogen, Tokyo, Japan). RT-PCR was performed using Maloney-murine leukemia virus (M-MLV) reverse transcriptase (Invitrogen) according to the manufacturer's instructions. Oligo-(dT19) primers (1.25 μM) and total RNA (10 μg) from the urinary bladders were heated to 65°C for 5 min. Then, 200 units M-MLV RT was added to a 20-μl reaction buffer containing 0.5 mM of each: deoxynucleotide triphosphate (dNTP; Operon, Tokyo, Japan), RNase inhibitor (40 units, Promega, Madison, WI), and 10 mM DTT (Invitrogen), and the reactions were incubated for 1 h at 37°C.

PCR was performed using an appropriate amount of the urinary bladder cDNA template in a 25-μl volume of Ex-Taq buffer containing 0.2 mM of each dNTP (Operon) and 0.5 μM of each of *primers 1* and *2* with 0.625 units of Ex-Taq polymerase (Takara, Kyoto, Japan). The PCR amplification procedure consisted of an initial denaturation step at 95°C for 5 min followed by 30 cycles of denaturation (94°C, 60 s), annealing (50°C, 60 s), and extension (72°C, 90 s) in a thermal cycler (ASTEC, Fukuoka, Japan). The PCR products were analyzed on a 2% agarose gel containing ethidium bromide (0.5 μg/ml) with Marker 6 (λ/*Sty* 1 digest; Wako Pure Chemicals, Osaka, Japan) as the molecular-weight marker. The products of interest were cut out of the gels, purified, and cloned into the pGEM-3Z vector (Promega) and then transformed into competent *Escherichia coli* JM 109 cells according to the supplier's instructions (Takara). The plasmid DNA was purified and sequenced.

Table 1. *Primers used for cloning and PCR analysis of Hyla AQPh3 BL sequence*

Name	Primer Sequence	
	AQP-h3BL	
Primer 1	5′-CTCATCCTKGTGATGTTYGG-3′	148–167 bp
Primer 2	5′-CCAGARTTGAAGCCCATGGA-3′	666–683 bp
Adaptor primer	5′-GACTCGAGTCGACATCGAT-3′	
	3′ RACE primers	
3′ Primer	5′-ATGGCTTGTACTATGAGCCC-3′	410–429 bp
3′ Nested primer	5′-GTGTCTTGGCCATTGTTGAC-3′	572–590 bp
	5′ RACE primers	
5′ Primer	5′-ACATAGAGCTGGTCGTTTGC-3′	442–461 bp
5′ Nested primer	5′-ATGAGGATACCCAGCATGAC-3′	250–269 bp

3′ and 5′ Rapid Amplication of cDNA End

Rapid amplication of cDNA end (RACE) technique was used to obtain the full-length Hyla AQP-h3BL mRNA sequence. For 3′-RACE, poly(A)$^+$ RNA was isolated from the total RNA using oligo(dT)-coated latex beads (Oligotex-dT30 super; Takara) according to the manufacturer's instructions. Isolated RNA was primed with oligo(dT19) adaptor primer and reverse-transcribed using M-MLV-RT, as described above. A 1-μl aliquot of the RT product was then PCR amplified with the 3′ primer and adaptor primer; subsequent amplification was performed using the 3′ nested primer and adaptor primer. Following denaturation at 95°C for 5 min, PCR amplification was carried out for five cycles (60 s at 94°C, 60 s at 60°C, 90 s at 72°C), five cycles (60 s at 94°C, 60 s at 58°C, 90 s at 72°C), five cycles (60 s at 94°C, 60 s at 56°C, 90 s at 72°C), and 15 cycles (60 s at 94°C, 60 s at 55°C, 90 s at 72°C). The clone obtained was subcloned and sequenced as described above.

For 5′-RACE, isolated RNA was primed with 5′ primer and reverse-transcribed using M-MLV-RT, as described above. This first strand of cDNA was purified with a QIA Quick PCR purification kit (Qiagen, Hilden, Germany); this purified first-stand cDNA for poly(A)$^+$ was added to 10 units of terminal deoxynucleotidyl transferase (TdT; Toyobo, Osaka, Japan) and purified once again using the kit. Using this purified first-stand cDNA, we then synthesized the second-strands of cDNA with Ex *Taq* polymerase (1.25 units) and oligo(dT19) adaptor primer sequentially for 5 min at 93°C, for 90 s at 42°C, and 3 min at 72°C. A 1-μl aliquot of second-strand cDNA was then amplified by PCR with the 5′ primer and adaptor primer. This product was then amplified by PCR with 5′ nested primer and adaptor primer. These PCR amplifications were carried out under conditions identical to those described for the 3′ RACE-PCR. The clone obtained was subcloned and sequenced as described below.

Nucleotide Sequence Analysis

The nucleotide sequences of cloned cDNAs or direct PCR cDNA products were determined by using an Aloka DNA sequencer [model Lic-4200L(S); Aloka, Tokyo, Japan].

Antibody

An oligopeptide corresponding to the COOH-terminal amino acids 283–292 (ST-184: LSNVKHKERI) of the Hyla AQP-h3BL, with an amino-terminal cysteine residue, was synthesized on a model 433A synthesizer (PE-Applied Biosystems, Foster City, CA). The crude peptide was purified by reverse-phase high-performance liquid chromatography with a 0–60% linear gradient of CH_3CN in 0.1% trifluoroacetic acid. Purification of the peptide was confirmed by measuring its molecular mass by mass spectrometry. The antibody was raised in a rabbit immunized with the ST-184 peptide coupled to keyhole limpet hemocyanin (Pierce, Rockford, IL), as described previously (33). The guinea pig anti-Hyla AQP-h2 (13), anti-Hyla AQP-h3 (35), and vacuole proton ATPase E-subunit (38) sera had been generated and characterized previously.

Western Blot Analysis

Several tissues, including the frog pelvic ventral skin, dorsal skin, urinary bladder, and kidney, heart, small intestine, lungs, liver, and

brain, were homogenized in cell lysis buffer (50 mM Tris·HCl, pH 8.0, 0.15 M NaCl, 1% Triton X-100, 0.1 mg/ml PMSF, 1 μg/ml aprotinin) and centrifuged at 12,000 rpm in a microcentrifuge for 10 min to remove insoluble materials. The protein was determined by using a BCA Protein Assay kit (Pierce). The supernatant protein (10 μg) was denatured at 70°C for 10 min in denaturation buffer comprising 3% SDS, 70 mM Tris·HCl, pH 6.8, 11.2% glycerol, 5% 2-mercaptoethanol, and 0.01% bromophenol blue, subjected to elec-

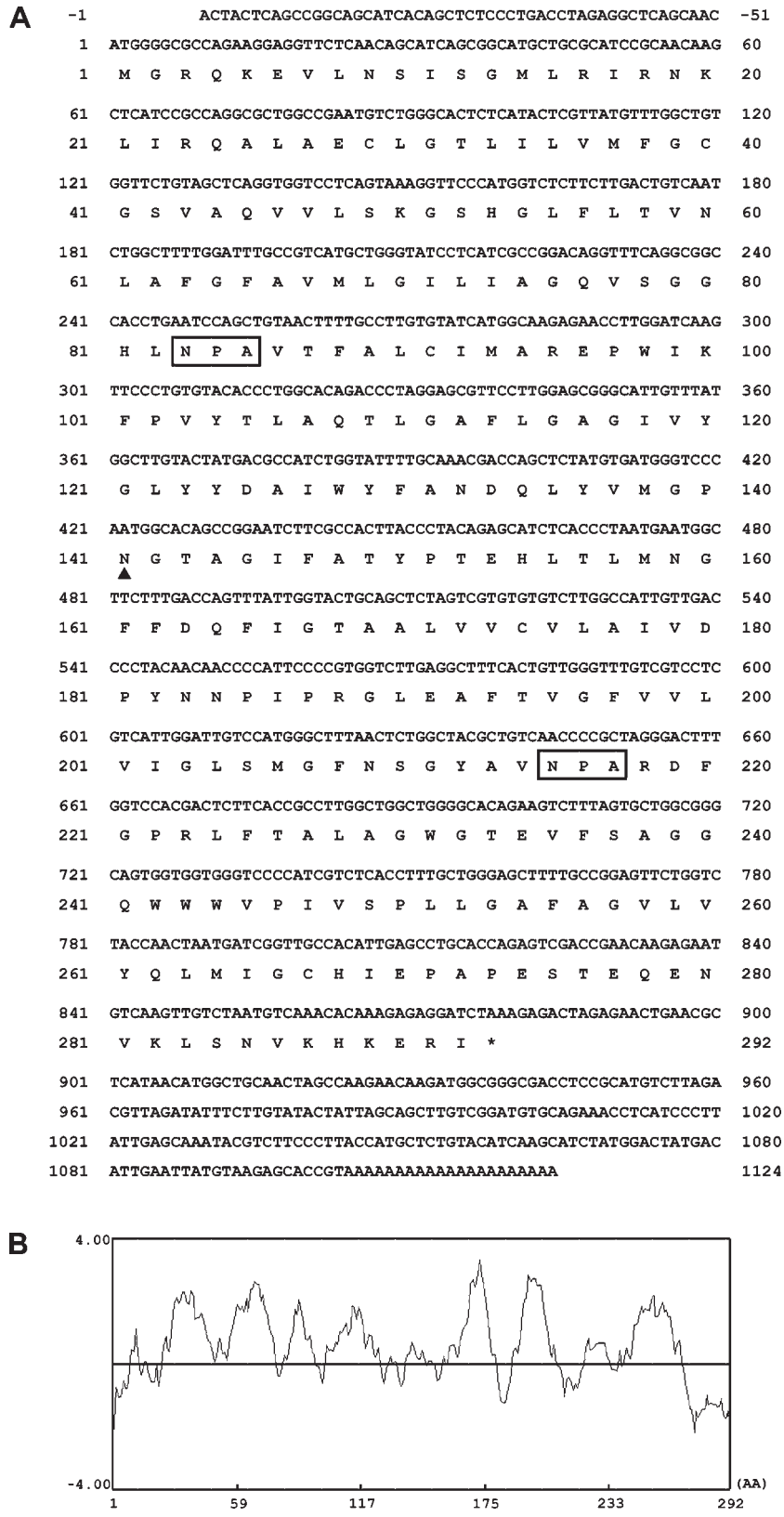

Fig. 1. *A*: nucleotide and deduced amino acid sequence of aquaporin (Hyla AQP-h3BL) cDNA. The predicted amino acid is shown below the nucleotide sequence. The asterisk indicates the terminal codon. Asn-Pro-Ala (NPA) motifs are outlined. The solid triangle indicates a putative N-glycosylation site. *B*: Kyte-Doolittle hydropathy profile (window 11) of the deduced AQP-h3BL amino acid sequence.

trophoresis on a 12% polyacrylamide gel, and then transferred to an Immobilon-P membrane (Millipore, Tokyo, Japan). The proteins on the membrane were reacted sequentially with anti-AQP-h3BL (ST-184) serum diluted at 1:5,000, biotinylated goat anti-rabbit IgG (DAKO, Kyoto, Japan), and streptavidin-conjugated horseradish peroxidase (DAKO). The reaction products on the membrane were visualized using an enhanced chemiluminescence Western blot detection kit (Amersham Pharmacia Botech, Buckinghamshire, UK). To check the specificity of the immunoreaction, we performed an absorption test by preincubating anti-AQP-h3BL (ST-184) with the antigen peptide (10 μg/ml). To determine whether the immunoreactive proteins were glycosylated, we treated the extracts from the ventral and dorsal skins, urinary bladders, and lungs at 37°C with peptide-N-glycosidase F (Daiichi Pure Chemicals, Tokyo, Japan) prior to SDS-PAGE and Western blot in accordance with the manufacturer's instructions. Similarly, AQP-h3BL proteins were compared between AVT-stimulated and nonstimulated pelvic skins. Five pieces of the pelvic skins were dissected and homogenized. After the supernatants had been measured for protein content, the samples (10 μg/lane) were analyzed by SDS-PAGE and Western blot analysis with anti-AQP-h3BL. The optical density of the Western blots was determined using NIH image software (version 1.62) on a Macintosh computer. The densitometry data were expressed as a percentage of the mean value for non-AVT-stimulated samples.

Osmotic Water and Glycerol Permeability of Oocytes

The full-length Hyla AQP-h3BL cDNA was produced by RT-PCR using the Kozak sequence with the Hyla AQP-h3BL-specific primer (5′-GCCGCCATGCTGAAATATTTTTTCTCTGGG-3′) and Hyla AQP-h3BL specific primer with poly(A)$_{25}$ [5′-(T)$_{25}$ACGGTGC-TCTTACATAATTCAAT-3′]. The product of PCR amplification was cloned into the pGEM-5Z vector (Promega). cRNAs were prepared from linearized pGEM-5Z vectors containing the entire open reading frame of AQP-h3BL by digestion with *Apa*I (Takara) and then transcribed and capped with SP6 RNA polymerase (mCAP RNA Capping kit, Stratagene, La Jolla, CA). *Stage V* and *VI Xenopus* oocytes were defolliculated by collagenase (1 mg/ml; Roche) and microinjected with either cRNAs (50 ng) or water. After a 3-day incubation in Barth's buffer at 18°C, the oocytes were transferred from 200 mOsm to 70 mOsm Barth's buffer, and the osmotically elicited increase in volume was monitored at 24°C under an Olympus BX50 microscope with a ×4 magnifying objective lens and a charge-coupled device (CCD) camera connected to a computer. The coefficient of osmotic water permeability (Pf) was calculated from the initial slope of oocyte swelling according to accepted methodology (8, 40). In some experiments, $HgCl_2$ was added to a final concentration of 0.3 mM for 10 min. To examine the recovery of the $HgCl_2$-induced inhibition by a reducing agent, oocytes were incubated for 10 min in Barth's buffer containing 5 mM β-mercaptoethanol following 10 min incubation in $HgCl_2$. To confirm whether AQP-h3BL protein was expressed in *Xenopus* oocytes following the injection of AQP-h3BL cRNA, we evaluated AQP-h3BL cRNA-injected or water-injected oocytes by Western blot analysis and immunostaining as described below. For the incorporation experiments, oocytes were incubated at room temperature in Barth's solution containing cold 1 mM glycerol and 2.5 μCi/ml of [U-^{14}C]glycerol (5.4 GBq/mmol; Amersham). Oocytes were removed from this medium after 0, 5, 15, and 30 min of incubation and rinsed five times in ice-cooled Barth's solution. The individual oocytes were lysed in 200 μl of 10% SDS overnight and the radioactivity measured by liquid scintillation counter (Aloka).

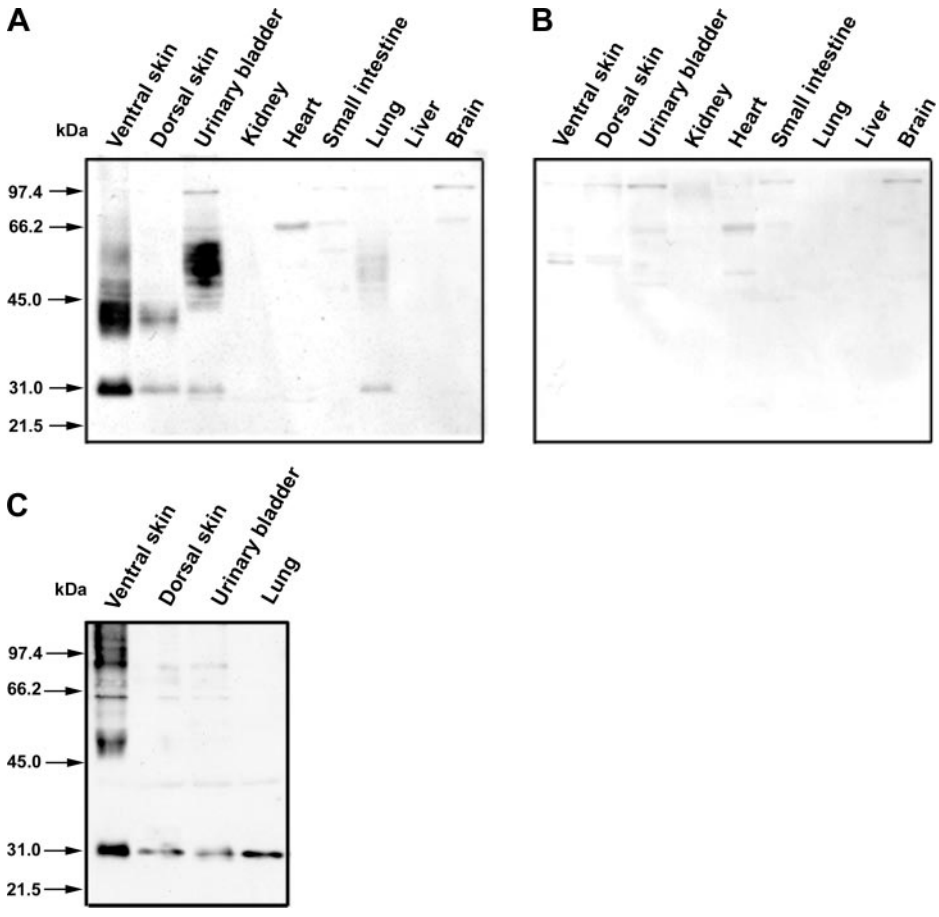

Fig. 2. *A*: Western blot analysis of extracts of several tissues using rabbit anti-Hyla AQP-h3BL. In the ventral and dorsal skins, urinary bladder, kidney, and lung, immunoreactive bands are seen at 31 kDa and at 40–65 kDa. The amount of the smear band at 40–65 kDa varies depending on the tissue. *B*: the membrane was immunostained with the antiserum preabsorbed with the immunogen peptide (10 μg/ml). Immunoreactive bands were completely abolished. Some nonspecific bands are visible in the area of the higher molecular masses. *C*: Western blot analysis of extracts of the ventral and dorsal skins, urinary bladder, and lungs after digestion of the extracts by peptide-N-glycosidase F. Specific bands with their extracts seen before digestion are replaced by a single band of 31 kDa, presumed to be the nonglycosylated form of Hyla AQP-h3BL, after digestion.

Immunofluorescence

The ventral and dorsal skins, urinary bladder, and kidney of the *Hyla* were fixed overnight at 4°C in periodate-lysine-paraformaldehyde fixative, dehydrated, and embedded in Paraplast. Thin (4 μm) sections were cut and mounted on gelatin-coated slides, deparaffinized, and rinsed with distilled water and PBS. For single labeling of AQP-h3BL protein, immunofluorescence staining was performed essentially as described previously (34). The sections were sequentially incubated with 1% BSA-PBS, rabbit anti-AQP-h3BL serum (1:2,000), and indocarbocyanine (Cy3)-labeled affinity-purified donkey anti-rabbit IgG (1:400; Jackson Immunoresearch, West Grove, PA). For nuclear counterstaining, 4′,6-diamidino-2-phenylindole (DAPI) was included in the secondary antibody solution. The sections were finally washed with PBS and then mounted in PermaFluor (Immunon, Pittsburgh, PA). The specificity of the immunostaining was checked using an absorption test by preincubating the anti-AQP-h3BL antiserum with the antigen peptide (10 μg/ml). For double-immunofluorescence staining for AQP-h3BL and AQP-h2 (ST-140; 13) or AQP-h3 (ST-141; 35), sections were first incubated with a mixture of rabbit anti-AQP-h3BL (1:2,000) and guinea pig anti-AQP-h2 (1:5,000; 13) or guinea pig anti-AQP-h3 (1:2,000; 13), and then reacted with a mixture of Cy3-labeled donkey anti-rabbit IgG (1:400; Jackson Immunoreseach) and Alexa Fluor 488-labeled goat anti-guinea pig IgG (1:200; Molecular probes, Eugene, OR), and DAPI. The stimulation experiments using AVT were carried out according to Hasegawa et al. (13). Some sections were double-stained for both AQP-h3BL and the bullfrog vacuolar H^+-ATPase E-subunit (V-ATPase; 38) to identify the renal tubules, urinary bladders, and skins (including the mucous glands), or for both AQP-h3BL and *Xenopus* AQP-x5 (21) to recognize the apical plasma membrane of the mucous glands. Specimens were examined with an Olympus BX50 microscope equipped with a BX-epifluorescence attachment (Olympus Optical, Tokyo, Japan).

Statistical Analysis

Statistical analysis was performed by using Student's *t*-test or Cochran-Cox test for nonhomogenous data.

RESULTS

cDNA Cloning of Hyla AQP-h3BL

Figure 1*A* shows the full cDNA sequence of Hyla AQP-h3BL and its deduced amino acid sequence. The cDNA consisted of a 51-bp 5′-untranslated region (UTR) and a 220-bp 3′-UTR followed by a poly(A) tail. An open reading frame encoded a protein of 292 amino acids with a relative molecular mass calculated at 31,530 kDa. Hydropath analysis predicted six transmembrane regions with an NH_2 terminus and a COOH terminus located in the cytoplasm, which is similar to other major intrinsic protein (MIP) family members (Fig. 1*B*). There was one putative N-linked glycosylation site at Asn-141. The amino acid sequence contained the conserved Asn-Pro-Ala (NPA) motif found in all MIP family members. The Hyla AQP-h3BL showed a high amino acid to its homologues in *Xenopus laevis* (87%; 30), mouse (80.5%; 20), human (80.8%; 18), chimpanzee (80.8%; XP520531), rat (80.4%; 17), Euro-

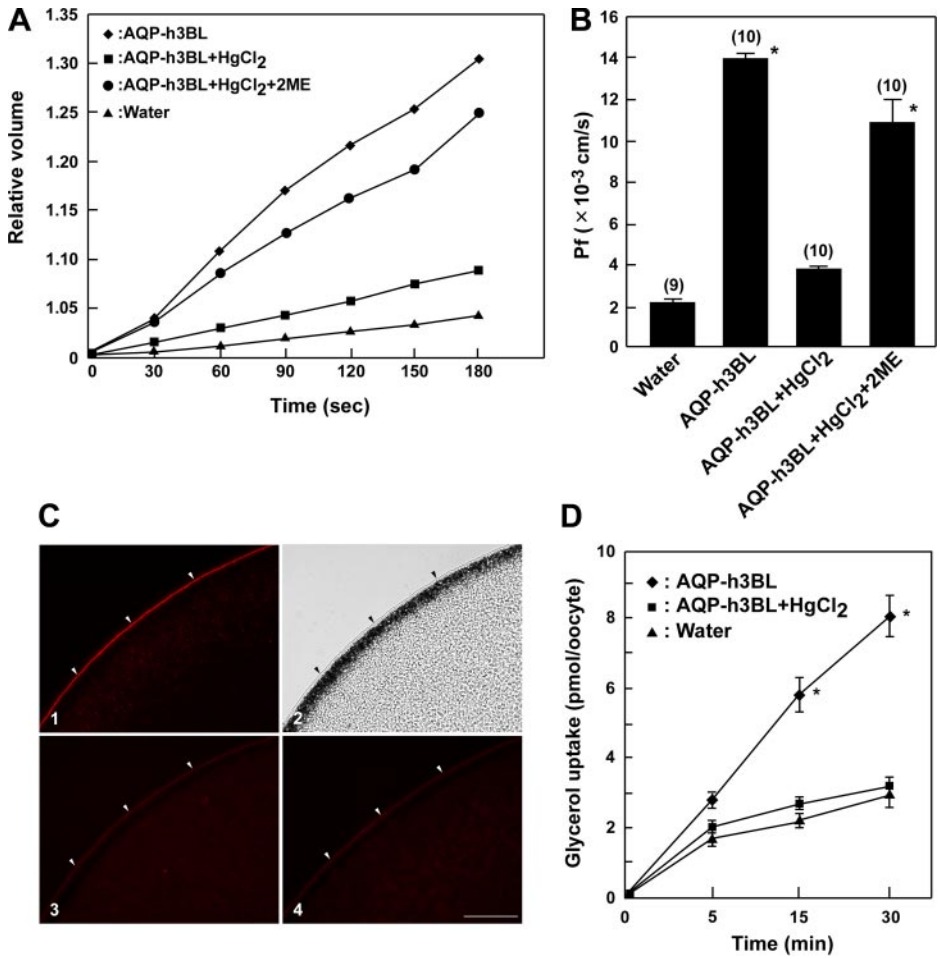

Fig. 3. Expression of AQP-h3BL in *Xenopus* oocytes. *A*: time course of the osmotic swelling. Oocytes were microinjected with water or cRNAs encoding AQP-h3BL. Some of the AQP-h3BL-injected oocytes were incubated with no additive, and some were incubated with 0.3 mM $HgCl_2$ or with 0.3 mM $HgCl_2$ followed by 5 mM β-mercaptoethanol (2ME). *B*: osmotic water permeability (Pf) was calculated from the initial rate of oocyte swelling. The representative data shown are given as the mean ± SE of measurements from 9 to 10 oocytes in each experimental group. $*P < 0.01$ vs. water. *C*: immunofluorescence images of the AQP-h3BL protein in AQP-h3BL-injected oocytes: after complete swelling of the oocytes, immunoreactive AQP-h3BL substances are visible, predominantly in the plasma membrane (*1*); the corresponding Nomarski differential interference image (*2*); in the absorption test, immunopositive substances obtained with anti-AQP-h3BL are nearly abolished at background levels in the AQP-h3BL-injected oocyte (*3*); and only background levels are observed in the water-injected oocyte with anti-AQP-h3BL (*4*). Arrowheads indicate the plasma membrane. Scale bar = 50 μm. *D*: time course of [^{14}C]glycerol uptake into oocytes injected with water or AQP-h3BL cRNA and 0.3 mM $HgCl_2$-treated oocytes with AQP-h3BL cRNA. Values are averaged as means ± SE from measurements of six oocytes at each point. $*P <$ 0.01 vs. water.

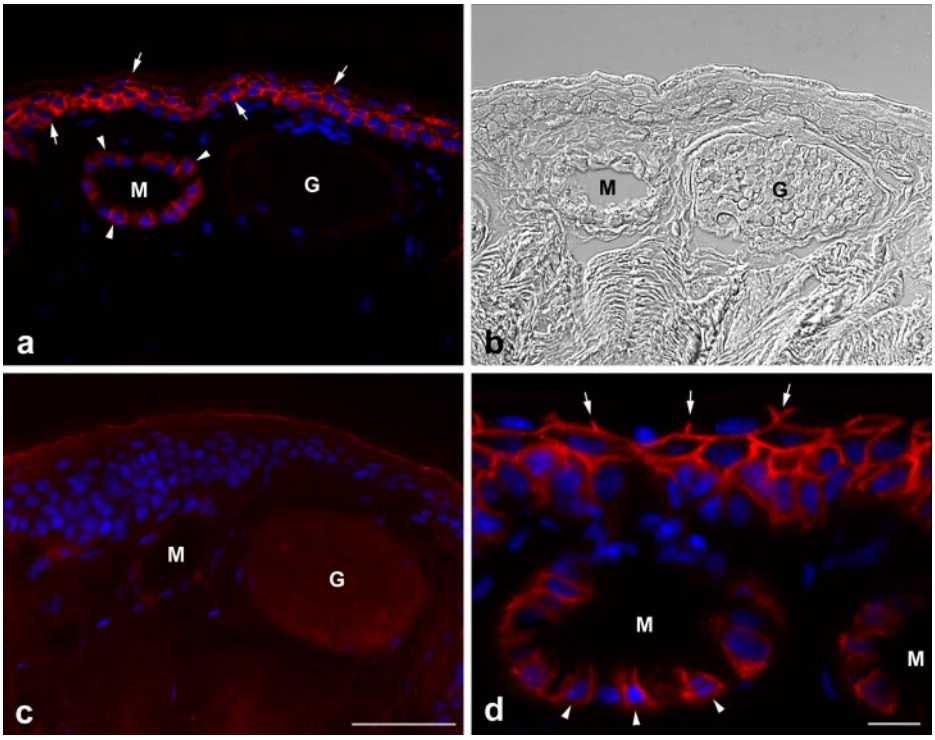

Fig. 4. Immunofluorescence localization of AQP-h3BL in the ventral pelvic skins. *a*, *c*, and *d*: Fluorescence images of AQP-h3BL. *b*: Corresponding Nomarski differential interference contrast image. *a* and *b*: Labels (red) are clearly visible in the basolateral plasma membrane of most granular cells (arrows) in the stratum granulosum and of the principal cells (arrowheads) in the mucous gland (M). No labeling is seen in the granular gland (G). Nuclei are counterstained with 4′,6-diamidino-2-phenylindole (DAPI; blue). *c*: No labeling is detected in any of the cells of the skins when anti-AQP-h3BL is preabsorbed with the corresponding antigen peptide. *d*: Enlarged view of AQP-h3BL-positive granular cells (arrows) in the stratum granulosum and principal cells (arrowheads) in the mucous gland. Note that the labelings is more intense in the granular cells of the stratum granulosum than in the secretory cells of the mucous gland. Scale bars: *a*, *b*, and *c* = 50 μm; *d* = 10 μm.

pean eel (72%; 4), tilapia (69.5%; 37), and *Ribolodon hakonensis* (67.8%; 16), as well as to Hyla AQP-h2 (64%; 12) and AQP-h3 (64%; 35). This sequence of full-length cDNA has been deposited in DDBJ/EMBL/GenBank (accession no. AB285019).

Western Blot Analysis of Several Tissue Preparations

To test the specificity of the antiserum for the skins, we carried out Western blot analysis of their extracts. In the extract of the ventral pelvic skins, the ST-184 antiserum detected a major band at about 31 kDa and a smear band between 40 and 65 kDa that was assumed to be glycosylated form (Fig. 2*A*). Similar bands were detected in the dorsal skin, urinary bladders, and lungs. A large amount of the glycosylated forms was found in the extract of the ventral pelvic and urinary bladders. No band was detected in the kidneys, heart, small intestine, liver, and brain. The bands described above were not detected when anti-Hyla AQP-h3BL was preabsorbed with the peptide used as the immunogen (Fig. 2*B*). After digestion with peptide-N-glycosidase F, the most-stained smear band became a band of 31 kDa, suggesting that the bands of apparent higher molecular mass represented glycosylated forms of the 31 kDa-Hyal AQP-h3BL protein (Fig. 2*C*).

Expression of Hyla AQP-h3BL in Xenopus Oocytes

Transmembrane water flow through the Hyla AQP-h3BL protein was evaluated by means of an expression analysis in *Xenopus* oocytes. After 3 days of incubation at 18°C, the oocytes were transferred from isotonic (200 mOsm) to hypoosmotic (70 mOsm) Barth's solution: swelling was monitored microscopically with an attached CCD camera, and the coefficient of Pf was subsequently calculated (Fig. 3*A*). The Pf of AQP-h3BL-injected oocytes was approximately sevenfold higher than that of water-injected oocytes. The stimulated water permeability was inhibited by 0.3 mM $HgCl_2$, and this inhibition was fully reversed by 5 mM β-mercaptoethanol treatment following the incubation in $HgCl_2$ (Fig. 3, *A* and *B*). When sections of the AQP-h3BL cRNA-injected oocytes were immunostained with anti-Hyla AQP-h3BL, a large immunofluorescent mass was observed in the plasma membrane (Fig.

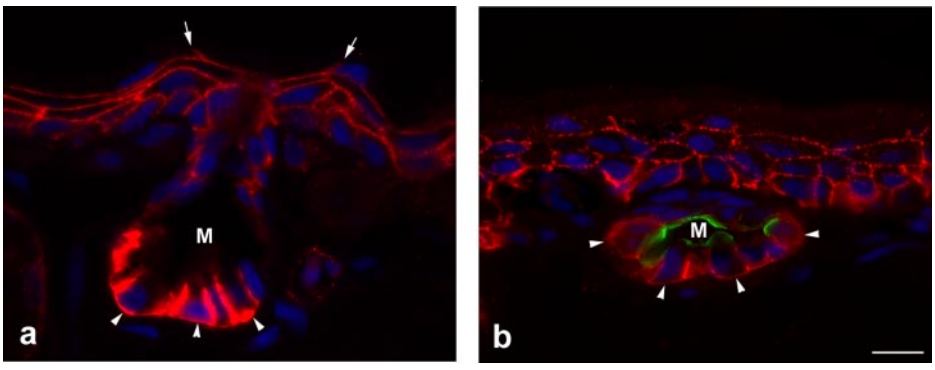

Fig. 5. Immunofluorescence localization of AQP-h3BL in the dorsal skins. *a*: Labels for AQP-h3BL are visible in the basolateral membrane of the granular cells (arrows) and of principal cells in the mucous gland (M; arrowheads). The labeling density is more intense in the basolateral plasma membrane of the principal cells of the mucous gland than in that of the granular cells in the skins. *B*: double-labeling of AQP-h3BL and AQP-x5. A second AQP, AQP-x5, is visible in the apical plasma membrane (green) of the secretory cells of the mucous gland, whereas AQP-h3BL is observed in the basolateral membrane (red: arrowheads) of the same cells. Nuclei are counterstained with DAPI (blue). Scale bar = 10 μm.

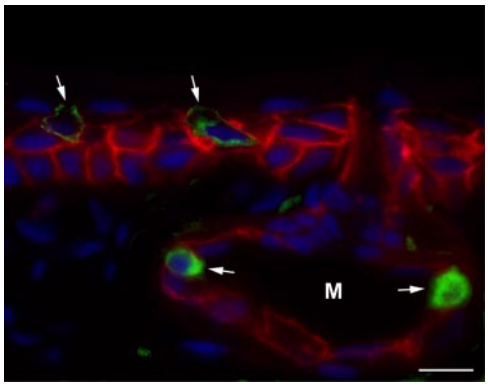

Fig. 6. Immunofluorescence localization of AQP-h3BL (red) and the V-ATPase E-subunit (green) in the skin. V-ATPase-positive cells, which are mitochondria-rich cells (arrows), do not stain with anti-AQP-h3BL. Nuclei are counterstained with DAPI (blue). Scale bar = 10 μm.

3*C*, *1* and *2*). The immunopositive sites were completely abolished followed by preabsorption of the antiserum with 10 μg/ml of the immunogen peptide (Fig. 3*C, 3*). The level of glycerol uptake in the AQP-h3BL-injected oocytes was higher than that in water-injected oocytes, and the glycerol uptake was inhibited by $HgCl_2$ (Fig. 3*D*).

Localization of Hyla AQP-h3BL in Several Osmoregulatory Tissues

Skins. The *Hyla* epidermis is organized into four successive layers: the stratum corneum, granulosum, spinosum, and germinativum, each of which consists of two main cell types: granular cells and mitochondria-rich (MR) cells. In some of the thin sections of these tissues, two types of exocrine glands were observed: granular and mucous glands. When the ventral pelvic skins were stained by the immunofluorescence method, Hyla AQP-h3BL protein was detected in several layers of the stratum granulosum, located just beneath the stratum corneum and the mucous gland (Fig. 4, *a* and *b*). To confirm the specificity of the labeling, we carried out a control experiment which showed that immunolabels for AQP-h3BL in the granular cells in the skin granular layers and the mucous glands were abolished when the antiserum was preincubated with the COOH-terminal peptide of AQP-h3BL protein used as the immunogen (Fig. 4*c*). In the stratum granulosum, AQP-h3BL was localized to the basolateral plasma membrane of most of the granular cells, but it was observed throughout the plasma membrane of the granular cells in the middle granular sublayer (Fig. 4*d*). In the dorsal skins, a similar pattern for AQP-h3BL was found in the basolateral plasma membrane in most of the granular cells in the stratum granulosum and in the secretory cells in the mucous glands (Fig. 5*a*). On the other hand, AQP-x5 protein, which was especially expressed in mucous glands, was present in the apical plasma membrane of secretory cells in the mucous glands, at the site at which water is secreted (21) (Fig. 5*b*). No signal was found in other types of cells including the MR cells, which could be identified based on the presence of the V-ATPase E-subunit (Fig. 6).

When the junction region between the pelvic and pectoral skins in the ventral side was stained with the AQP-h3BL antiserum, the distribution of the intensity of the label remained constant throughout all of the regions from the pelvic to the pectoral skin, whereas the labels for AQP-h2 or AQP-h3 decreased in a gradient from the pelvic skin toward the pectoral skin, suggesting that the AQP-h3BL protein is expressed throughout the entire skins (Fig. 7). This observation was confirmed by comparing the amount of AQP-h3BL protein expressed in AVT-stimulated and nonstimulated ventral pelvic skins by means of Western blot analysis. AVT-stimulated ventral pelvic skins showed 100.0 ± 2.5 (n = 5) expression units, which the nonstimulated one showed 104.2 ± 2.1 (n = 5), this difference was nonsignificant.

Following stimulation of the frog ventral pelvic skins by AVT, the granular cells were labeled with AQP-h3BL together with AQP-h2 or AQP-h3. AQP-h2 and AQP-h3 were observed in the apical plasma membrane. Conversely, in the nonstimulated frogs AQP-h2- and AQP-h3-positive reactions were seen primarily in the cytoplasm (Fig. 8).

Urinary bladders. The urinary bladder of the frog consists of a transitional epithelium supported by a thin layer of connective tissue. Two cell types are mainly recognized in this epithelium: granular cells and MR cells. When the urinary bladder was immunostained with the AQP-h3BL antiserum, the label was observed in the basolateral plasma membrane of the granular cells (Fig. 9, *a, b,* and *d*). No labeling of the urinary bladder was obtained when the antiserum was preabsorbed with its corresponding immunogen (Fig. 9*c*). In addition, the intensity of double labels for the AQP-h3BL and V-ATPase E-subunit, with the latter used as a specific marker in MR cells, was found to be different in different cells of the urinary bladder: AQP-h3BL was primarily expressed in the principal cells and V-ATPase was found predominantly in the MR cells (Fig. 10). Following AVT stimulation, AQP-h2 was located to the apical region of the plasma membrane, whereas

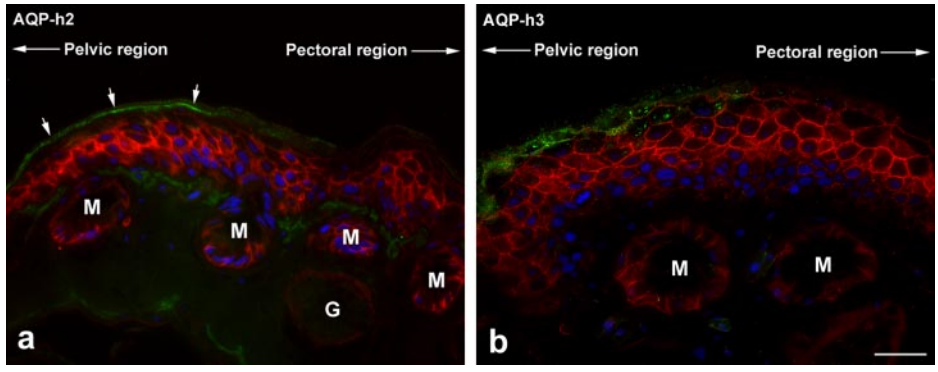

Fig. 7. Immunofluorescence localization of AQP-h3BL and AQP-h2 (*a*) or AQP-h3 (*b*) in the ventral skins. The labeling density for AQP-h2 (green: arrows) or AQP-h3 (green: arrows) gradually decreases from the pelvic skin to the pectoral skin. In contrast, the label for AQP-h3BL (red) is clearly visible over the entire surface from the ventral to pectoral skins. Nuclei are counterstained with DAPI (blue). Scale bar = 50 μm.

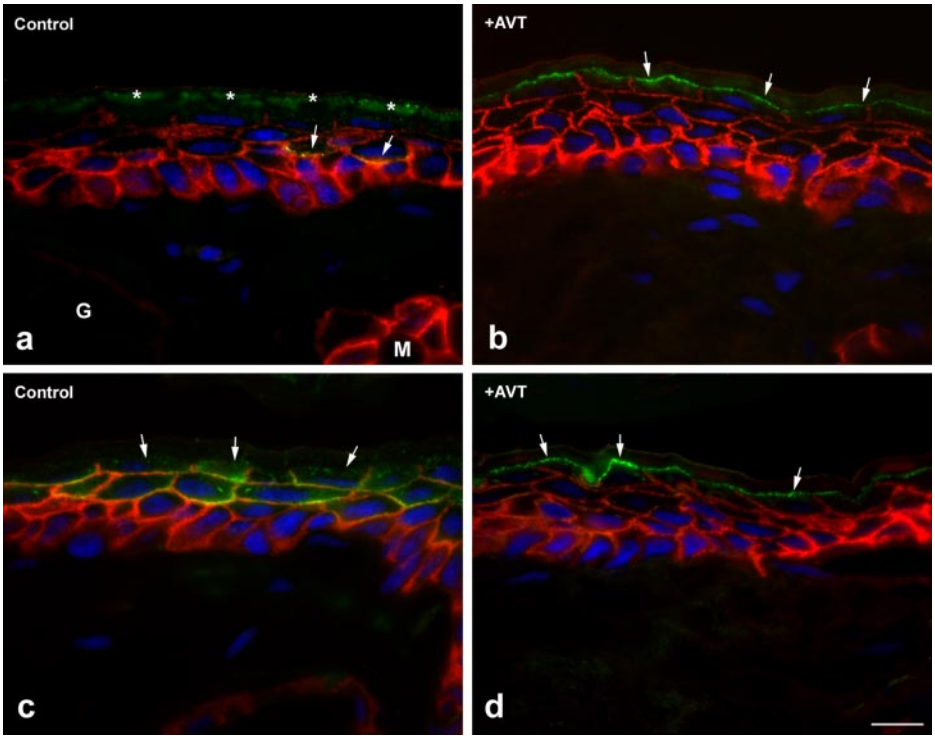

Fig. 8. Double-immunofluorescence micrographs showing the granular cells in the ventral pelvic skins labeled for AQP-h3BL and AQP-h2 or AQP-h3 under nonstimulated and arginine vasotocin (AVT)-stimulated conditions. a and b: Immunolabeling results for AQP-h3BL (red) and AQP-h2 (*a*) or AQP-h3 (*c*) under the nonstimulated condition. Immunolabeling results for AQP-h3BL (red) and AQP-h2 (*b*) or AQP-h3 (*d*) in response to vasotocin. Upon stimulation of AVT, the labelings for AQP-h2 and AQP-h3 (green: arrows) moved from the cytoplasm to the apical plasma membrane in the outermost part of the sublayer of stratum granulosum. However, the labels for AQP-h3BL are similarly expressed in the basolateral membrane of the granular cells before and after AVT stimulation. Nuclei are counterstained with DAPI (blue). *Keratinized layers. Scale bar = 10 μm.

AQP-h3BL is expressed in the basolateral plasma membrane, as well as controls (Fig. 11). These results confirmed those of a previous study that reported that AQP-h2 is mainly located to the cytoplasm (14).

Kidneys. According to Uchiyama and Yoshizawa (36), the anuran nephrons are divided into eight parts, including a glomerulus, a proximal tubule, a late distal tubule, a collecting duct, and a neck segment. When kidney sections were labeled with anti-AQP-h3BL, the labels were seen in the collecting ducts and part of the late distal tubule (Fig. 12, *a* and *b*). When sections of the frog kidneys were stained with the preabsorbed antiserum with the antigen (10 μg/ml), immunopositive labels were abolished (Fig. 12*c*). Immunopositive labels were observed in the basolateral plasma membrane of the principal

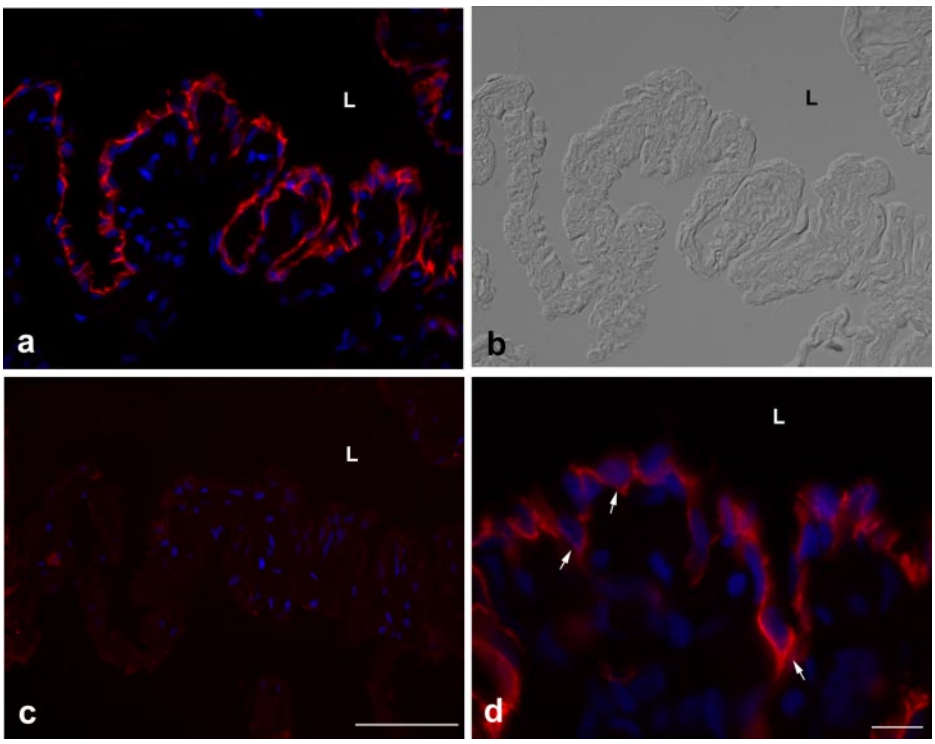

Fig. 9. Immunofluorescence localization of AQP-h3BL in the urinary bladder. *a*, *c*, and *d*: Fluorescence images of AQP-h3BL. *b*: Corresponding Nomarski differential interference contrast image. *a* and *b*: Labels (red) are clearly visible in the basolateral plasma membrane of principal cells in the urinary bladder. Nuclei are counterstained with DAPI (blue). *c*: No labeling is detected in any of the cell of the skins when anti-AQP-h3BL is preabsorbed with the corresponding antigen peptide. *d*: Enlarged view of AQP-h3BL-positive basolateral plasma membrane (red; arrows) in the principal cells. L, lumen. Scale bars: *a*, b, and c = 50 μm; *d* = 10 μm.

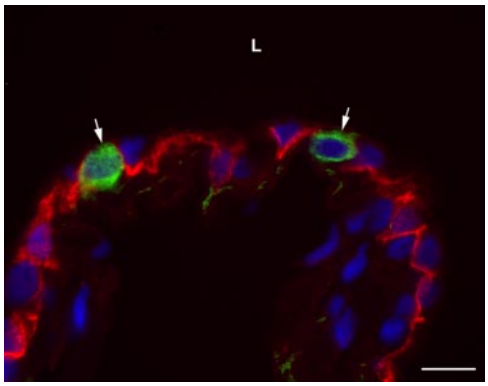

Fig. 10. Double-immunofluorescence images for AQP-h3BL and V-ATPase E-subunit in the urinary bladder. The labels for AQP-h3BL (red) are not visible in the V-ATPase-positive cells (green; arrows). Nuclei are counterstained with DAPI (blue). Scale bar = 10 μm.

cells of both tubules (Fig. 12*d*). The AQP-h3BL-positive cells were different from the V-ATPase-positive MR cells, and we were therefore able to use the number of MR cells as the criterion for distinguishing between the collecting ducts and the late distal tubule (Fig. 13).

DISCUSSION

We report here the full sequence of an mRNA encoding an AQP that is specifically expressed in the basolateral plasma membrane of several osomregulatory organs in the tree frogs, namely, skins, urinary bladders, and kidneys. This AQP (denoted AQP-h3BL) was structurally characterized as having two NPA motifs and six putative transmembrane domains. Interestingly, this AQP-h3BL does not have a cysteine at a mercurial sensitivity site just upstream of the second NPA motif, but it was still able to significantly inhibit water permeability, as well as mammalian AQP3 in *Xenopus* oocytes as revealed by the standard oocyte swelling assay. This Hg^{2+}-induced inhibition was restored by β-mercaptoethanol, the reducing agent that may dissociate Hg^{2+} from AQP. Thus, the inhibition by Hg^{2+} was not due to nonspecific toxicity of mercury compounds, but was a reversible phenomenon. Mammalian AQP3 have six cysteine residues at positions 11, 29, 40, 91, 174, and 267; in comparison, Hyla AQP-h3BL also has cysteine residues at identical positions with the expectation of position 11. Based on results from site-directed mutagenesis studies, Kuwahara et al. (22) reported that of these six cyteine residues, Cys-11 is the mercury-sensitive site. In Hyla AQP-h3BL, the Cys-11 is replaced by isoleucine; however, Hyla AQP-h3BL has shown to be sensitive to mercury. The AQP3 proteins in tilapia (37), European eel (4), and Japanese dace (16) have also substituted isoleucine for Cys-11 and, in addition, the water permeability of tilapia AQP3 proteins are significantly inhibited by $HgCl_2$ (37). It would therefore appear that Cys-11 is not an absolute requirement for inhibition of water permeability, a conclusion that is contradictory to the results reported by Kuwahara et al. (22).

The first NPA motif changes to NPT in AQP3 of European eel (4) and Zebrafish (NP-998633). Hyla AQP-h3BL contained NPAVT and NPARD sequences, which are characteristic sequences conserved among proteins of the aquaporin family, as well as a sequence homologous to glycerol facilitator of *E. coli* (6, 19).

A homology analysis revealed that the deduced amino acid sequence of AQP-h3BL has a high degree of homology to mammalian AQP3. Furthermore, AQP-h3BL had a putative N-linked glycosylation site at Asn-141, but no putative phosphorylation site for protein kinase A.

Water- and glycerol-permeability experiments using *Xenopus* oocytes revealed that AQP-h3BL facilitates water and glycerol permeation and that $HgCl_2$ inhibits both these abilities, suggesting that this AQP-h3BL can be classified as a member of the aquaglyceroporin subfamily within the AQP family. Interestingly, Zimmerman et al. (41) indicated that AQP3 (HC-3) cloned from the liver of Cope's gray tree frog (*Hyla chrysoscelis*) is permeable to both water and glycerol and that the water and glycerol uptake balance is dependent upon the temperature of the environment; a higher uptake of glycerol was observed at 10°C than at 23°C, whereas the reverse relation was observed with water uptake. This functional change in AQP3 (HC-3) has been proposed as the new regulatory system of AQP.

The Western blot analysis and digestion experiments with peptide-N-glycosidase F of the extract of *Hyla* skin, urinary bladder, and lungs showed that AQP-h3BL protein was present in nonglycosylated and glycosylated forms. We also clearly showed that this antibody (ST-184) was specific for the tree frog AQP-h3BL protein because the preabsorbed antiserum stained only nonspecific bands. The molecular mass of the nonglycosylated form is in good agreement with the predicted molecular mass (~31 kDa) based on the amino acid sequence of AQP-h3BL protein. Although we were unable to detect any bands for AQP-h3BL in the kidney by Western blot analysis, immunopositive reactions were obtained by immunofluores-

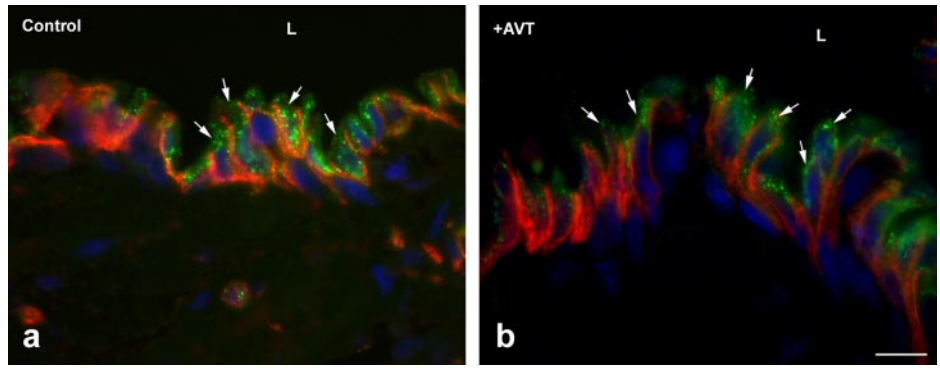

Fig. 11. Double-immunofluorescence micrographs showing the granular cells in the urinary bladder labeled for AQP-h3BL and AQP-h2 under nonstimulated and vasotocin-stimulated conditions. Immunolabeling results for AQP-h3BL and AQP-h2 under the nonstimulated condition (*a*) and in response to vasotocin (*b*) are shown. Upon stimulation of AVT, the labels for AQP-h2 (green; arrowheads) moved from the cytoplasm to the apical plasma membrane in the principal cells. However, the labels for AQP-h3BL remained evenly constant in the basolateral membrane of the granular cells before and after the AVT stimulation. Nuclei are counterstained with DAPI (blue). Scale bar = 10 μm.

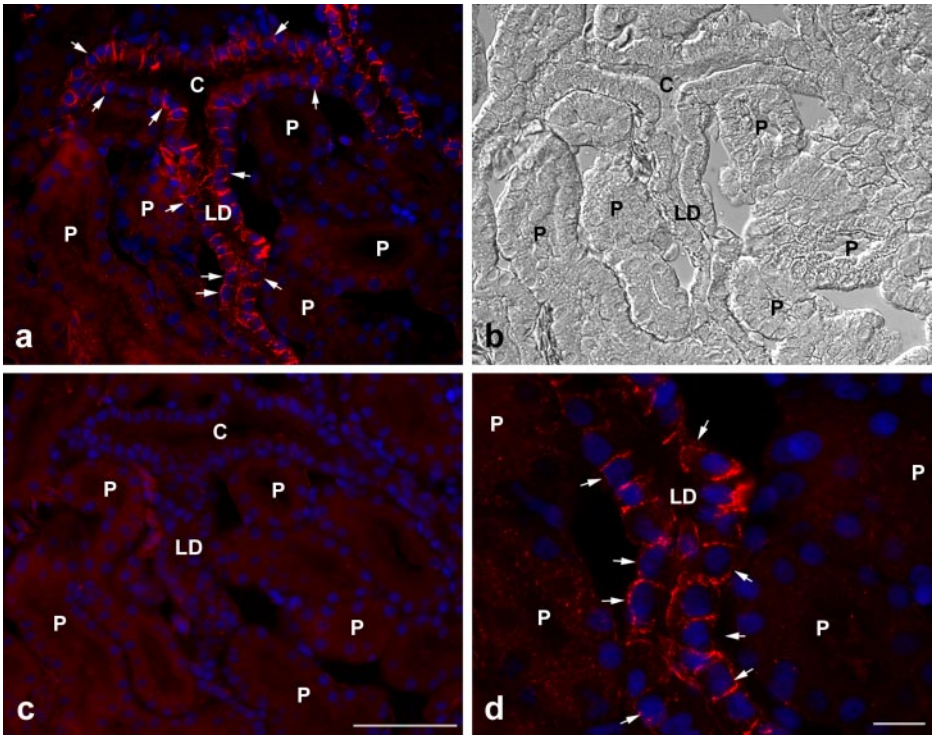

Fig. 12. Immunofluorescence localization of AQP-h3BL in the kidney. *a*, *c*, and *d*: Fluorescence images of AQP-h3BL. *b*: Corresponding Nomarski differential interference contrast image. *a* and *b*: Labels (red; arrowheads) are clearly visible in the basolateral plasma membrane of the principal cells in the collecting ducts (C) and in the late distal tubules (LD). No labeling is visible in other parts including the proximal tubules (P). *c*: No labeling is detected in any of the cells of the kidney when anti-AQP-h3BL is preabsorbed with the corresponding antigen peptide. *d*: Enlarged view of AQP-h3BL-positive principal cells in the kidney. The labels are in the basolateral plasma membrane (arrowheads). Nuclei are counterstained with DAPI (blue). Scale bars: *a*, *b*, and *c* = 50 μm; *d* = 10 μm.

cence with the same antiserum, and this fluorescence was abolished when the corresponding antigen peptide was used for adsorption. It would therefore appear that this antiserum is specific to AQP-h3BL in the kidney. AQP-h3BL proteins were present with varying amounts of glycans in each the tissues: a large amount of glycans in the ventral skins and urinary bladders and less in the dorsal skins. In addition, a previous investigation also showed a large amount of glycosylated form of AQP-h2 in the urinary bladder (12). These differences in the amount of glycans of the AQP in each tissue have not fully been explained, but it is known that the glycosylated and nonglycosylated forms for mammalian AQP2 protein. Human AQP2-T125M, a mutant that causes recessive nephrogenic diabetes insipidus (9, 26), is not glycosylated because the consensus N-linked glycosylation motif is disrupted. Interestingly, this protein is absent in the plasma membrane (26). It is therefore important to clarify the underlying molecular mechanisms for the movement of the glycosylated form of AQP2 to the plasma membrane. Hendriks et al. (15) have demonstrated that N-linked glycosylation is important for the transport of molecules from the Golgi complex and the sorting of AQP2 to the plasma membrane: in their experiments, nonglycosylated AQP2-N123Q protein was not delivered to the cell surface in the MDCK-AQP2-N123Q cells. Thus, the glycosylation of mammalian AQP2 is crucial for translocation to the plasma membrane; however, other AQPs, including *Xenopus* AQP-x5, have no consensus N-glycosylation site, and their AQPs are still expressed in the plasma membrane (21). One likely possibility is that only mammalian AQP2 protein may have this glycosylation requirement for translocation to the cell membrane.

Our immunofluorescence study revealed that AQP-h3BL was expressed in the ventral and dorsal skins, urinary bladders, and kidneys based on the presence of anti-Hyla AQP-h3BL label in the basolateral plasma membrane of granular cells in the stratum granulosum of the whole frog body. This labeling pattern is similar to localization of mammalian AQP3 protein observed by Matsuzaki et al. (27), who reported the localization of mammalian AQP3 protein to the basolateral plasma membrane of the basal and intermediate cell layers in the

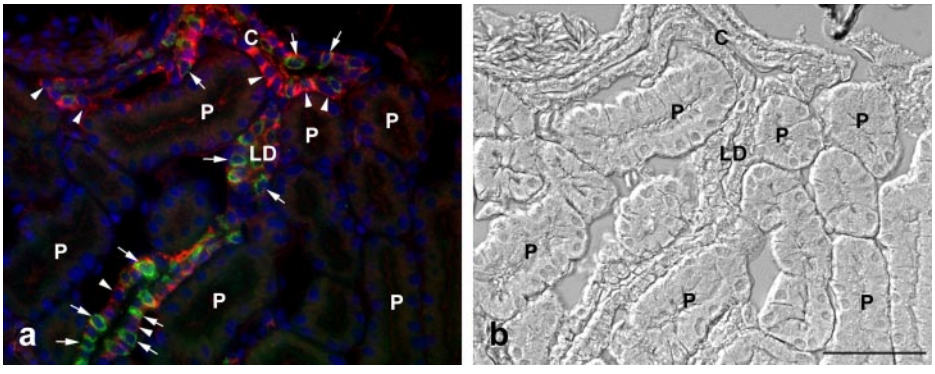

Fig. 13. Double-immunofluorescence images for AQP-h3BL and V-ATPase E-subunit in the kidney. The labels for AQPh3BL are different from those for the V-ATPase E-subunit. The V-ATPase-positive cells (green; arrows) is more numerous in a portion of late distal tubules (LD) than in the collected ducts (C). Nuclei are counterstained with DAPI (blue). Scale bar = 50 μm.

epidermis. Matsuzaki et al. (27) proposed that AQP3 in epidermal cells functions as finely tuned machinery to supply water to the water-deprived epidermal cells from the underlying dermis where capillaries provide enough water from the blood. Ma et al. (25) reported that water and glycerol permeability was reduced in the epidermis of the AQP3-null mice. Furthermore, surface conductance measurement showed a remarkable reduction of the water content of the keratinized layer. Based on these results, these authors concluded that AQP3 protein plays a pivotal role in hydration of the epidermis, especially in keratinized layer. Hara et al. (10) found that the content of water and glycerol in the keratinized layer in the AQP3-null mice was reduced to half of that found in control wild-type mice. Since AQP3 is permeable to glycerol, as well as water, the selective reduction of glycerol content in AQP3-null mice in the epidermis and keratinized layer may account for these defects. AQP3 is a critical determinant in supplying glycerol to the epidermis, and a sufficient amount of glycerol in the epidermis is important for maintaining the hydration and healthy condition of the epidermis (11). Because frog skins are exposed directly to external environments, which is a completely different situation from that found in other animals, the evaporation of water through the skin is much higher in frogs. AQP-h2 and AQP-h3 are specifically expressed in the ventral pelvic skins, where water absorption occurs (12, 35). These AQP proteins are translocated to the apical plasma membrane in response to stimulation by AVT for the purpose of absorbing water through the membrane, whereas the water that exited from the cytoplasm through the AQP-h3BL protein will move to capillaries via the connective tissues. The AQP-h3BL protein is constitutively expressed in the basolateral plasma membrane, thereby supporting the results of our Western blot analysis data showing there were no significant differences in the amount of AQP-h3BL protein between AVT-stimulated and nonstimulated ventral pelvic skins. In addition to localization of AQP-h3BL protein in the basolateral membrane, we previously showed that both AQP-h2 and AQP-h3 proteins are located at the basolateral plasma membrane of the first-reacting granular cells in the nonstimulated ventral pelvic skin of the tree frogs (13). It is an interesting issue to determine whether AQP-h2BL, AQP-h2, and AQP-h3 are colocalized on the plasma membrane and intracellular vesicles. Immunoelectron microscopic study will be required for defining roles of each AQP in the water absorption of the ventral pelvic skins.

We also found that AQP-h3BL protein was present in the basolateral plasma membrane of secretory cells in mucous glands, as revealed by the presence of labeled AQP-x5, which is homologous to mammalian AQP5, in the apical membrane of these secretory cells (21). Consequently, water is absorbed through the AQP-h3BL protein from the underlying connective tissues and is secreted through the AQP-x5 protein from the apical membrane to the body surfaces. The frog mucous glands therefore play an important role in the secretion of water by providing a moisture texture in the body surfaces and by regulating body temperatures via evaporation heat (23).

We found that AQP-h3BL protein was also present in the basolateral plasma membrane of the principal cells in the urinary bladder; these cells could be distinguished from the MR cells based on the expression of the V-ATPase E-subunit in the latter. Similar to the ventral pelvic skins, AQP-h2 protein pooled in the cytoplasm moved to the apical plasma membrane of the principal cells in the urinary bladder in response to AVT-stimulation. The AQP-h2 protein expressed in the apical membrane absorbs water from the lumen of the urinary bladder; this water will then move through the AQP-h3BL to the connective tissues and then to the capillaries.

The present study clearly demonstrated that immunopositive cells were present among the principal cells of the collecting ducts and a portion of the late distal tubules of the kidneys. This difference between the collecting ducts and late distal tubules is recognized by the difference in the number of MR cells in these two tissues of the kidneys: there are relatively few MR cells in the principle cell of collecting ducts and many more MR cells in the late distal tubules. However, we should not dismiss the possibility of the presence of an AVT-dependent AQP in the apical plasma membrane, despite the fact that the existence of just such an AQP has not been empirically demonstrated. However, Zimmerman et al. (41) have recently cloned a cDNA encoding an AQP-like 2 protein (HC-2) from Cope's gray tree frog (*Hyla chrysoscelis*), and we also have cloned a similar AQP (Hyla AQP-h2K) from the kidney of *Hyla japonica* (Y. Ogushi, H. Mochida, T. Nakakura, M. Suziki, and S. Tanaka, unpublished data). Thus, these AQPs may be specific to the kidney (kidney-type of AQP) and expressed in the apical plasma membrane in an AVT-dependent manner. Suzuki et al. (31) demonstrated the presence of two AQP groups in anuran amphibians by drawing a phylogenetic tree: one AQP is depicted as belonging mammalian AQP2 family containing Hyla AQP2 (HC-2) (41) and Hyla AQP-h2K (Y. Ogushi, H. Mochida, T. Nakakura, M. Suziki, and S. Tanaka, unpublished data), and the other is shown to be pelvic- and urinary-type AQP.

In conclusion, the results reported here demonstrated that AQP-h3BL protein is expressed in the basolateral plasma membrane in concert with AVT-dependent or AVT-independent AQP in several epithelial cells of various anuran osmoregulatory organs where it has crucial functions in water homeostasis.

ACKNOWLEDGMENTS

We thank Kenji Ishibashi, Molecular Biology, Clinical Research Center, Chiba-east Hospital, Chiba, Japan, for teaching the procedure to glycerol incorporation.

GRANTS

This investigation was supported in part by a grant-in-aid for scientific research from the Ministry of Education, Science, Sports, and Culture of Japan (to S. Tanaka).

REFERENCES

1. **Agre P.** The aquaporin water channels. *Proc Am Thorac Soc* 3: 5–13, 2006.
2. **Bentley PJ.** The Amphibia. In*: Endocrines and Osmoregulation. A Comparative Account in Vertebrates*, vol. 39, edited by Bentley PJ, New York: Springer, 2002, p. 155–186.
3. **Brown D.** Membrane recycling and epithelial cell function. *Am J Physiol Renal Fluid Electrolyte Physiol* 256: F1–F12, 1989.
4. **Cutler CP, Cramb G.** Branchial expression of an aquaporin 3 (AQP-3) homologue is downregulated in the European eel *Anguilla anguilla* following seawater acclimation. *J Exp Biol* 205: 2643–2651, 2002.
5. **Ecelbarger CA, Terris J, Frindt G, Echevarria M, Marples D, Nielsen S, Knepper MA.** Aquaporin-3 water channel localization and regulation in rat kidney. *Am J Physiol Renal Fluid Electrolyte Physiol* 269: F663–F672, 1995.

6. **Echevarria M, Windhager EE, Tate SS, Frindt G.** Cloning and expression of AQP3, a water channel from the medullary collecting duct of rat kidney. *Proc Natl Acad Sci USA* 91: 10997–11001, 1994.
7. **Frigeri A, Gropper MA, Turck CW, Verkman AS.** Immunolocalization of the mercurial-insensitive water channel and glycerol intrinsic protein in epithelial cell plasma membranes. *Proc Natl Acad Sci USA* 92: 4328–4331, 1995.
8. **Fushimi K, Uchida S, Hara Y, Hirata Y, Marumo F, Sasaki S.** Cloning and expression of apical membrane water channel of rat kidney collecting tubule. *Nature* 361: 549–552, 1993.
9. **Goji K, Kuwahara M, Gu Y, Matsuo M, Marumo F, Sasaki S.** Novel mutations in aquaporin-2 gene in female siblings with nephrogenic diabetes insipidus: evidence of disrupted water channel function. *J Clin Endocrinol Metab* 83: 3205–3209, 1998.
10. **Hara M, Ma T, Verkman AS.** Selectively reduced glycerol in skin of aquaporin-3 deficient mice may account for impaired skin hydration, elasticity and barrier recovery. *J Biol Chem* 277: 46616–46621, 2002.
11. **Hara M, Verkman AS.** Glycerol replacement corrects defective skin hydration, elasticity, and barrier function in aquaporin-3-deficient mice. *Proc Natl Acad Sci USA* 100: 7360–7365, 2003.
12. **Hasegawa T, Tanii H, Suzuki M, Tanaka S.** Regulation of water absorption in the frog skins by 2 vasotocin-dependent water-channel aquaporins, AQP-h2 and AQP-h3. *Endocrinology* 144: 4087–4096, 2003.
13. **Hasegawa T, Sugawara Y, Suzuki M, Tanaka S.** Spatial and temporal expression of the ventral pelvic skin aquaporins during metamorphosis of the tree frog, *Hyla japonica*. *J Membr Biol* 199: 119–126, 2004.
14. **Hasegawa T, Suzuki M, Tanaka S.** Immunocytochemical studies on translocation of phosphorylated AQP-h2 protein in granular cells of the frog urinary bladder before and after stimulation with vasotocin. *Cell Tissue Res* 322: 407–415, 2005.
15. **Hendriks G, Koudijs M, van Balkom BW, Oorschot V, Klumperman J, Deen PM, van der Sluijs P.** Glycosylation is important for cell surface expression of the water channel aquaporin-2 but is not essential for tetramerization in the endoplasmic reticulum. *J Biol Chem* 279: 2975–2983, 2004.
16. **Hirata T, Kaneko T, Ono T, Nakazato T, Furukawa N, Hasegawa S, Wakabayashi S, Shigekawa M, Chang MH, Romero MF, Hirose S.** Mechanism of acid adaptation of a fish living in a pH 3.5 lake. *Am J Physiol Regul Integr Comp Physiol* 284: R1199–R1212, 2003.
17. **Ishibashi K, Sasaki S, Fushimi K, Uchida S, Kuwahara M, Saito H, Furukawa T, Nakajima K, Yamaguchi Y, Gojobori T, Marumo F.** Molecular cloning and expression of a member of the aquaporin family with permeability to glycerol and urea in addition to water expressed at the basolateral membrane of kidney collecting duct cells. *Proc Natl Acad Sci USA* 91: 6269–6273, 1994.
18. **Ishibashi K, Sasaki S, Saito F, Ikeuchi T, Marumo F.** Structure and chromosomal localization of a human water channel (AQP3) gene. *Genomics* 27: 352–354, 1995.
19. **Ishibashi K, Kuwahara M, Sasaki S.** Molecular biology of aquaporins. *Rev Physiol Biochem Pharmacol* 141: 1–32, 2000.
20. **Kishida K, Kuriyama H, Funahashi T, Shimomura I, Kihara S, Ouchi N, Nishida M, Nishizawa H, Matsuda M, Takahashi M, Hotta K, Nakamura T, Yamashita S, Tochino Y, Matsuzawa Y.** Aquaporin adipose, a putative glycerol channel in adipocytes. *J Biol Chem* 275: 20896–20902, 2000.
21. **Kubota M, Hasegawa T, Nakakura T, Tanii H, Suzuki M, Tanaka S.** Molecular and cellular characterization of a new aquaporin, AQP-x5, specifically expressed in the small granular glands of *Xenopus* skin. *J Exp Biol* 209: 3199–3208, 2006.
22. **Kuwahara M, Gu Y, Ishibashi K, Marumo F, Sasaki S.** Mercury-sensitive residues and pore site in AQP3 water channel. *Biochemistry* 36: 13973–13978, 1997.
23. **Lillywhite HB.** Temperature selection by the bullfrog, *Rana catesbeiana*. *Comp Biochem Physiol A* 40: 213–227, 1971.
24. **Ma T, Frigeri A, Hasegawa H, Verkman AS.** Cloning of a water channel homolog expressed in brain meningeal cells and kidney collecting duct that functions as a stilbene-sensitive glycerol transporter. *J Biol Chem* 269: 21845–21849, 1994.
25. **Ma T, Hara M, Sougrat R, Verbavatz JM, Verkman AS.** Impaired stratum corneum hydration in mice lacking epidermal water channel aquaporin-3. *J Biol Chem* 277: 17147–17153, 2004.
26. **Marr N, Bichet DG, Hoefs S, Savelkoul PJ, Konings IB, De Mattia F, Graat MP, Arthus MF, Lonergan M, Fujiwara TM, Knoers NV, Landau D, Balfe WJ, Oksche A, Rosenthal W, Muller D, Van Os CH, Deen PM.** Cell-biologic and functional analyses of five new Aquaporin-2 missense mutations that cause recessive nephrogenic diabetes insipidus. *J Am Soc Nephrol* 13: 2267–2277, 2002.
27. **Matsuzaki T, Suzuki T, Koyama H, Tanaka S, Takata K.** Water channel protein AQP3 is present in epithelial exposed to the environment of possible water loss. *J Histichem Cytochem* 47: 1275–1286, 1999.
28. **Nielsen S, Chou CL, Marples D, Christensen EI, Kishore BK, Knepper MA.** Vasopressin increases water permeability of kidney collecting duct by inducing translocation of aquaporin-CD water channels to plasma membrane. *Proc Natl Acad Sci USA* 92: 1013–1017, 1995.
29. **Park JH, Saier MH Jr.** Phylogenetic characterization of the MIP family of transmembrane channel proteins. *J Membr Biol* 153: 171–180, 1996.
30. **Schreiber R, Pavenstadt H, Greger R, Kunzelmann K.** Aquaporin 3 cloned from *Xenopus laevis* is regulated by the cystic fibrosis transmembrane conductance regulator. *FEBS Lett* 475: 291–295, 2000.
31. **Suzuki M, Hasegawa T, Kubota M, Ogushi Y, Tanaka S.** Amphibian aquaporins and adapation to terrestrial environments. A review. *A Mol Integr Physiol*. In press.
32. **Takata K, Matsuzaki T, Tajika Y.** Aquaporins: water channel proteins of the cell membrane. *Prog Histochem Cytochem* 39: 1–83, 2004.
33. **Tanaka S, Kurosumi K.** A certain step of proteolytic processing of proopiomelanocortin occurs during the transition between two distinct stages of secretory granules maturation in rat anterior pituitary corticotrophs. *Endocrinology* 131: 779–786, 1992.
34. **Tanaka S, Yora T, Nakayama K, Inoue K, Kurosumi K.** Proteolytic processing of pro-opiomelanocortin occurs in acidifying secretory granules of AtT-20 cells. *J Histochem Cytochem* 45: 425–436, 1997.
35. **Tanii H, Hasegawa T, Hirakawa N, Suzuki M, Tanaka S.** Molecular and cellular characterization of a water channel protein, AQP-h3, specifically expressed in the frog ventral skin. *J Membr Biol* 188: 43–53, 2002.
36. **Uchiyama M, Yoshizawa H.** Nephron structure and immunohistochemical localization of ion pumps and aquaporins in the kidney of frogs inhabiting different environments. In: *Osmoregulation and Drinking in Vertebrates*, edited by Hazon N and Flik G. Oxford, UK: BIOS Scientific Publishers, 2002, p. 109–128.
37. **Watanabe S, Kaneko T, Aida K.** Aquaporin-3 expressed in the basolateral membrane of gill chloride cells in Mozambique tilapia *Oreochromis mossambicus* adapted to freshwater and seawater. *J Exp Biol* 208: 2673–2682, 2005.
38. **Yajima S, Kubota M, Nakakura T, Hasegawa T, Katagiri N, Tomura H, Sasayama Y, Suzuki M, Tanaka S.** Cloning and expression of the vacuolar proton-pumping ATPase subunits in the follicular epithelium of bullfrog endolymphatic sac. *Zool Sci*. 24: 147–157.
39. **Yamamoto T, Sasaki S, Fushimi K, Ishibashi K, Yaoita E, Kawasaki K, Marumo F, Kihara I.** Vasopressin increases AQP-CD water channel in apical membrane of collecting duct cells in Brattleboro rats. *Am J Physiol Cell Physiol* 268: C1546–C1551, 1995.
40. **Zhang RB, Logee KA, Verkman AS.** Expression of mRNA coding for kidney and red cell water channels in *Xenopus* oocytes. *J Biol Chem* 265: 15375–15378, 1990.
41. **Zimmerman SL, Frisbie J, Goldstein DL, West J, Rivera K, Krane CM.** Excretion and conservation of glycerol, and expression of aquaporins and glyceroporins, during cold acclimation in Cope's gray tree frog, *Hyla chrysoscelis*. *Am J Physiol Regul Integr Comp Physiol* 292: R544–R555, 2007.